Mechanisms of O_2 sputtering from water ice by keV ions

B. D. Teolis, R. A. Vidal, J. Shi, and R. A. Baragiola
University of Virginia, Laboratory for Atomic and Surface Physics, Engineering Physics, Charlottesville, Virginia 22904, USA
(Received 24 August 2005; revised manuscript received 24 October 2005; published 22 December 2005)

We have conducted experiments on the sputtering of water ice by 100 keV Ar^+ between 20 and 150 K. Our findings indicate that the temperature dependence of the total sputtering yield is heavily influenced by the thermal and irradiation history of the ice, showing a complex dependence on irradiation fluence that is correlated to the ejection of O_2 molecules. The results suggest that O_2 produced by the ions inside the ice diffuses to the surface where it is trapped and then ejected via sputtering or thermal desorption. A high concentration of O_2 can trap in a subsurface layer during bombardment at 130 K, which we relate to the formation of hydrogen and its escape from that region. A simple model allows us to determine the depth profile of the absolute concentration of O_2 trapped in the ice.

DOI: 10.1103/PhysRevB.72.245422 PACS number(s): 61.80.Jh, 79.20.−m, 96.35.Er, 96.35.Hv

I. INTRODUCTION

The surfaces of airless objects in the outer solar system are subject to continual irradiation by the solar wind and magnetospheric plasmas. The discovery of abundant H_2O on these surfaces created considerable interest in the response of water ice to energetic ion bombardment. Initial studies by Brown *et al.*[1] revealed that mega-electron-volt protons erode water ice surfaces by sputtering much more efficiently than anticipated for conventional elastic, or knock-on, sputtering mechanisms[2,3] important in metals and semiconductors. These workers showed that the sputtering yield of ice (number of molecules ejected per projectile ion) is proportional to the square of the electronic stopping power $S_e=dE/dx$,[4,5] meaning that sputtering can be induced by energy transfers via electronic excitations. In addition, ion irradiation of molecular solids can lead to the formation of new molecules[6,7] through bond breaking and reformation. Such radiation products have been detected in the sputtered flux of several condensed gases.[8–11] In water ice, the primary species sputtered, in addition to H_2O, are H_2 and O_2.[6,8,12–15] The latter is the probable source of the tenuous oxygen atmospheres reported at Europa[16–20] and Ganymede,[17–19,21] and of O^+ and O_2^+ detected in Saturn's magnetosphere.[19,22–24]

The sputtering yields of H_2 and O_2 show a strong temperature dependence over a broad range of temperatures. An increase in D_2 and O_2 sputtering from D_2O ice with temperature was demonstrated for 1.5 MeV He^+ (Ref. 12) and 30 keV Kr^+ (Ref. 9) from 20 to 150 K, and the same was shown in O_2 sputtering from H_2O ice with 100 keV Ar^+ (Ref. 25) and 200 keV H^+ (Ref. 26). It has been suggested that the temperature dependence arises from a thermally activated process, such as diffusion of O_2 or its precursors, or chemical interactions between precursor species.[12,14,27] Experiments have also shown that the O_2 yield is *negligible* for 1.5 MeV Ne^+ ions on D_2O ice at zero fluence, but increases asymptotically with fluence to a temperature-dependent saturation level.[12,14] Therefore individual ions do not eject O_2 from ice samples that were not previously irradiated, suggesting that a chemical transformation is required to enable O_2 ejection by later ions.[12,14,20] Past experiments determined that the O_2 yield returns to its previous value following interruptions of a few minutes in the ion flux,[12,14] implying that the transformation is permanent on this time scale at the temperatures tested. Boring *et al.*[12] and Reimann *et al.*[14] postulate that the increase in O_2 yield with fluence is related to the accumulation of O_2 in the ice matrix, and thermal desorption measurements have verified that O_2 is produced and *retained* in water ice by irradiation with 200 keV protons.[26] This trapped oxygen has been suggested to be a source for the condensed O_2 identified in the icy surfaces of Europa and Ganymede.[20,28–30] More recent models propose that rather than being due to the accumulation of trapped O_2, the fluence dependence in the O_2 sputtering yield is due to the production and accumulation of trapped precursor species[20] such as H_2O_2 or O atoms.[31,32] The present study was undertaken to quantify the fluence dependence of O_2 sputtering from ice, with the aim of establishing the viability of different precursor models.

II. EXPERIMENTS

Experiments were performed in a cryopumped ultrahigh vacuum chamber with a base pressure of 10^{-10} Torr. Water ice films were vapor deposited through a microcapilary doser onto a gold-coated quartz-crystal microbalance attached to a liquid helium cryostat, and cooled to as low as 20 K. The mass per unit area of the condensed films was determined by measuring the shift in the resonance frequency of the quartz crystal during deposition.[33] Films were deposited at 100 K to a thickness of 8500 monolayers (ML), where 1 ML is defined as 10^{15} molecules/cm^2. Samples were irradiated at 45 deg incidence by 100 keV Ar^+, which penetrate ~500 ML below the ice surface.[34] The ion beam was scanned over a circular 5 mm diameter collimating aperture to ensure uniform irradiation of the samples. The beam current was measured with a Faraday cup and the ion flux was maintained close to 2.7×10^{11} Ar^+/cm^{2}s. This current was nearly the same as measured on the gold substrate, indicating negligible charging of the ice films. A quadropole mass spectrometer, positioned normally to the sample surface, was used to measure fluxes of sputtered H_2O and O_2. Since the sputtered flux is predominantly neutral,[14] the mass spectrometer was operated

with the electron impact ionizer turned on. $H_2{}^{18}O$ ices were used to permit distinction of the sputtered species from background $H_2{}^{16}O$ and $^{16}O_2$ in the vacuum system.

To assure that the signals of H_2O and O_2 at the mass spectrometer were proportional only to the sputtered flux, without contributions from the ambient partial pressures of H_2O and O_2 in the vacuum chamber, the mass spectrometer was mounted in a separate stainless steel enclosure pumped by an ion pump. The enclosure was connected to the main chamber via a 2.5 mm diameter, 5 mm long tube, positioned 3 cm in front of the sample allowing entrance to molecules ejected normally to the ice surface. More details of this setup are given in Ref. 35. The mass spectrometer signal for species i is $\propto \gamma_i t_i Q_i + \beta_i P_i$, where Q denotes the flux entering the enclosure by way of the tube, t is the time of passage through the ionizer for molecules *initially* entering the enclosure, P is the background pressure for molecules not detected on the first pass through the ionizer, and γ and β are sensitivity factors. Since $P_i = Q_i / S_i$, where S is the pumping speed of the ion pump, the signal of species i is $\propto Q_i$, that is, proportional to the flux of sputtered species i in the normal direction. Since t is inversely proportional to the speed at which the sputtered molecules pass through the ionizer which in principle depends on the temperature of the sample, the factor relating Q to the sputtered flux is also temperature dependent. Due to small instabilities in the beam current, the signals were normalized to the beam current after background subtraction to obtain accurate yields for sputtered H_2O and O_2.

The reduction of the mass of the films due to sputtering was monitored with the microbalance. The rate of change in mass with irradiation fluence is converted to the number of molecules ejected per incident ion Y, or sputtering yield, using

$$Y = -\frac{1}{M}\frac{dm}{d\phi}, \tag{1}$$

where m is the mass per unit area, ϕ is the fluence, and M is the molecular mass of the sputtered species. When the sputtered flux consists of several species, Eq. (1) gives the *total* sputtering yield in units of mass M, but not the relative contributions of different species to the sputtered flux. In this paper, we use $M = 20$ amu when using Eq. (1) to give total sputtering yields from microbalance data in terms of $H_2{}^{18}O$ molecular masses. This is equal to the true $H_2{}^{18}O$ yield when $H_2{}^{18}O$ is the dominant species sputtered. In general, however, the relative contributions of individual species to the sputtered flux must be determined using the mass spectrometer.

III. RESULTS AND DISCUSSION

A. Dependence of the sputtering yield on sample history

We began our studies with an examination of the temperature dependence of the total sputtering yield of water ice by 100 keV Ar^+. Several 8500 ML films were deposited at 100 K and taken to different temperatures, where they were irradiated to fluences of $\sim 10^{15}$ Ar^+/cm^2. The average total sputtering yields at 20, 100, and 130 K, calculated from the *cumulative* mass loss of the films, are shown in Fig. 1. Little change is seen in the total sputtering yield from 20 to 100 K, but a sharp increase is observed above 100 K. This is consistent with previous results for other ions and energies.[9,12,19,25,36] Also shown in Fig. 1 are the total sputtering yields for one particular film, deposited at 100 K, then taken to different temperatures and irradiated with $1\text{-}2 \times 10^{15}$ Ar^+/cm^2 each time. The arrows indicate changes in temperature to illustrate the history of the film. Curiously, the sputtering yields for this film deviate from those of fresh films when the temperature is changed.

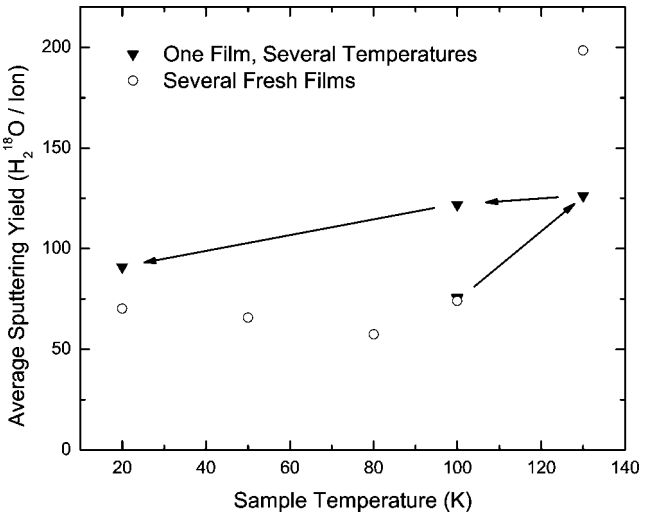

FIG. 1. Open circles: Total sputtering yields (in $H_2{}^{18}O$ molecules/ion) for 100 keV Ar^+ at 45 deg incidence onto fresh $H_2{}^{18}O$ films. Solid triagles: Sputtering yields of a previously irradiated film. Arrows indicate change in temperature between irradiations for previously irradiated ice to demonstrate the hysteresis behavior.

Evidently, the ice films retain a "memory" of past irradiations at other temperatures. Nonetheless, this memory is eventually lost, for if the total irradiation fluence is increased, at any temperature, the average total sputtering yield approaches asymptotically that for an initially fresh film. This indicates that the sputtering yield is not constant, but a function of irradiation fluence. Figure 2 shows the sputtering yield versus fluence calculated from the *instantaneous* rate of mass loss for the single film experiment of Fig. 1. As shown in Fig. 2(a) the total sputtering yield for the freshly deposited film irradiated at 100 K was roughly constant at $\sim$73 molecules/ion. However, the sputtering yield exhibited an intriguing transient behavior when the film was taken to 130 K and irradiated, starting at $\sim$115, decreasing fast to $\sim$95, then slowly rising to a saturation at $\sim$145 [Fig. 2(b)]. Then, when the film was cooled back to 100 K and irradiated once more, as in Fig. 2(c), the sputtering yield increased with fluence to a level in excess of that of Fig. 2(a). Finally, when the film was cooled to 20 K and irradiated, another striking transient in the sputtering yield occurred [Fig. 2(d)] with a fast rise followed by a slow decline.

Figure 3 shows an experiment similar to that of Fig. 2, but without an initial irradiation at 100 K. Again, the total sput-

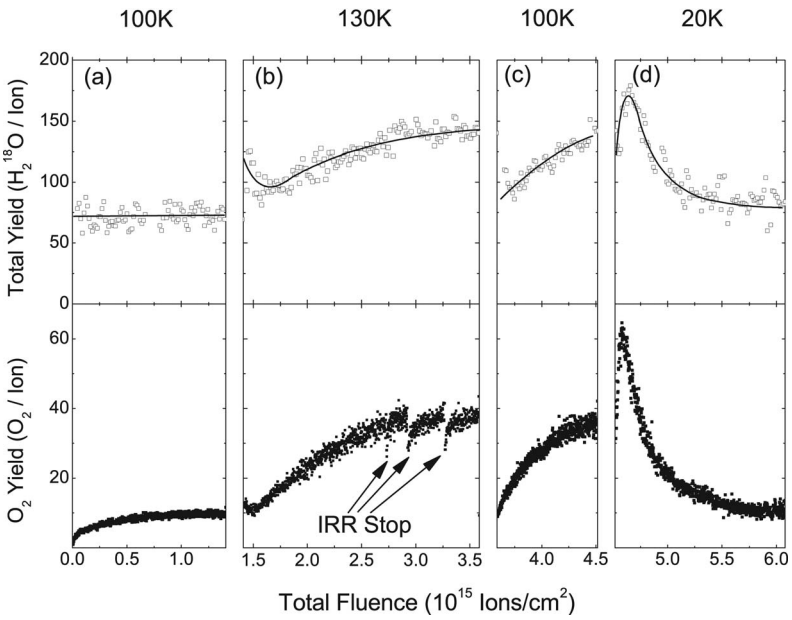

FIG. 2. (a) Total sputtering yield and O_2 yield versus fluence for 100 keV Ar^+ irradiation of fresh film at 100 K. (b) Film of (a) warmed to 130 K and irradiated. IRR Stop denotes interruption of several minutes in irradiation. (c) Film of (b) cooled to 100 K and irradiated. (d) Film of (c) cooled to 20 K and irradiated.

tering yield shows remarkable transient behaviors, but with some differences from those of Fig. 2.

B. Correlation to the O_2 yield

Using the mass spectrometer, we found that the partial H_2O yield is independent of fluence at temperatures in the range of 20–130 K. However, the O_2 yield, also shown in Figs. 2 and 3, exhibited transient behavior. For fresh films at any temperature [e.g., Figs. 2(a) and 3(a)] the O_2 yield was initially zero, rising with fluence to a saturation value, in general agreement with the previous 1.5 MeV Ne^+ results.[12,14] We observed no dependence of the saturation O_2 yield on the ion flux between 2×10^{11} and 1.5×10^{12} Ar^+/cm^2s. However, the O_2 yield was sensitive to the history of the film, and exhibited more elaborate transient behavior when previously irradiated films were irradiated at different temperatures, similar to that of the total sputtering yield. This indicates that the transients in the total sputtering yields were caused by the contribution of O_2 emission to the mass loss, which is consistent with previous conclusions that ejected O_2 can constitute a significant fraction of the species sputtered from water ice.[9,12,25,26] Therefore, we have normalized the mass spectrometer data for O_2 to account for the mass loss measured with the microbalance, which leads to the O_2 yield scales given in Figs. 2 and 3.

With sufficiently high irradiation fluences, the ice loses all memory of its history. Consequently, all O_2 yields should eventually approach the same temperature-dependent saturation levels, irrespectective of the history of the ice. Yet the apparent saturation of the O_2 yield for the 100 K irradiation of Fig. 2(c) is inconsistent with this picture, since it is greater than that of Fig. 2(a). Accordingly, the experiment of Fig. 2 was repeated, but with three times more irradiation fluence

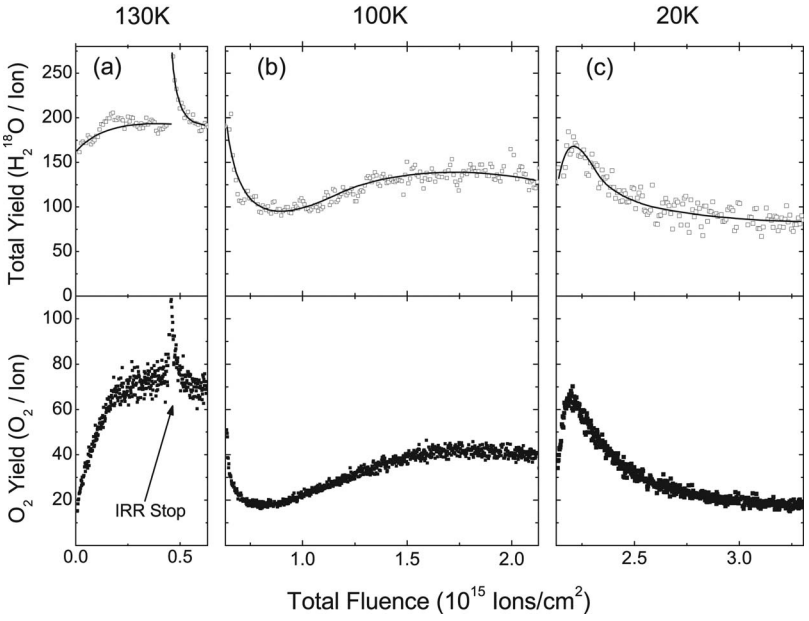

FIG. 3. (a) Total sputtering yield and O_2 yield versus fluence for 100 keV Ar^+ irradiation of a fresh film at 130 K. IRR Stop denotes interruption of 14 min in irradiation. (b) Film of (a) cooled to 100 K and irradiated. (c) Film of (b) cooled to 20 K and irradiated.

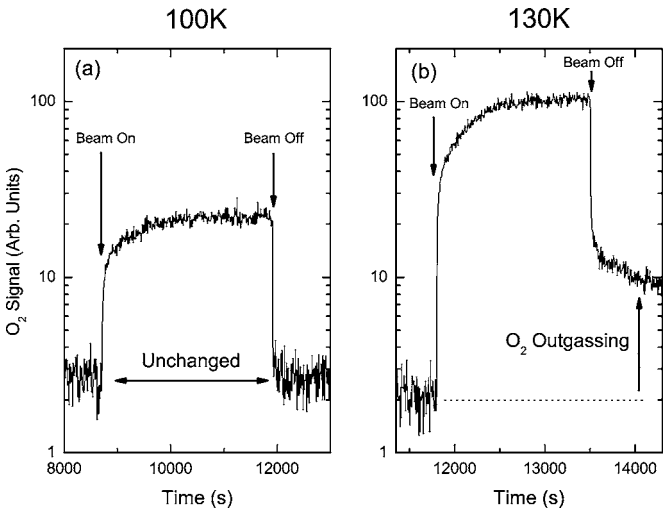

FIG. 4. O_2 signal at mass spectrometer versus time during irradiation of fresh film with 100 keV Ar^+ at (a) 100 K; (b) 130 K.

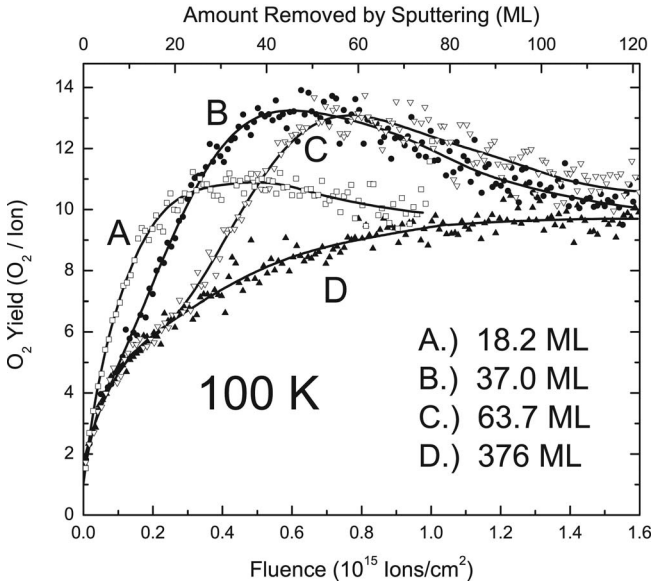

FIG. 5. Mass spectrometer data showing O_2 yield versus fluence and monolayers removed by sputtering for unirradiated ice overlayers deposited atop an 8500 ML (monolayers) film previously irradiated to O_2 yield saturation. Curve D is identical to that of a fresh film. The experiment was done at 100 K.

for the second 100 K irradiation. As anticipated, the O_2 yield initially rose, but then gradually dropped toward the expected saturation value. A similar drop was observed when the 100 K irradiation of Fig. 3(b) was done to greater fluence.

C. Time-dependent effects

At 20 and 100 K, we have found that the O_2 yield returns to the same value if the irradiation is terminated and then reinitiated after several minutes. This was true for fresh films and previously irradiated films, and also for the previous 1.5 MeV Ne^+ results.[12,14] However, at 130 K, the O_2 yield does not return to its previous value when ion irradiation is stopped and restarted, as in Figs. 2(b) and 3(a). For fresh films irradiated at 130 K, as in Fig. 3(a), interruption of irradiation after O_2 yield saturation initially caused a *higher* O_2 yield that quickly dropped back to the previous saturation value. Repeated interruptions in the ion beam caused the same behavior. Moreover, the longer the interruptions, the higher the initial O_2 yield on continuation of the irradiation. By contrast, interruptions in 130 K irradiations of ices previously irradiated at temperatures of 100 K or below initially produced a *lower* O_2 yield on continuation of the irradiation, whereupon the yield rose back to the previous saturation value. This behavior is noted in Fig. 2(b).

Irradiation at 130 K also induced outgassing of O_2 from the ice, which persisted even after the irradiation was interrupted. Figure 4 compares the O_2 signal plotted versus time for 2.7×10^{11} Ar^+/cm^2s irradiations of fresh films at 100 and 130 K. One can see that at 100 K, O_2 emission occurred only during irradiation, ceasing promptly when the irradiation was terminated. The same was true at lower temperatures, irrespective of irradiation history. However, at 130 K [Fig. 4(b)], O_2 emission did *not* cease after the irradiation was discontinued. The same effect was observed at 130 K for films previously irradiated at 100 K. We recall that Bahr *et al.*[26] and Baragiola and Bahr[37] found that 200 keV H^+ irradiation of ice produces trapped O_2 in addition to O_2 sputtering, and that trapped O_2 gradually escapes from water ice by thermal diffusion. The result of Fig. 4 can be understood similarly: Irradiation at 130 K produces trapped O_2, which then diffuses out thermally.

D. Effect of overlayers and radiation-induced diffusion

Since thermal diffusion of trapped O_2 occurs at 130 K, we sought to determine if diffusion is responsible for the history-dependent transient behaviors in the O_2 yield observed at 100 and 20 K. Benit and Brown have demonstrated the effect of *radiation-induced* diffusion of O atoms on the transient behavior of the O_2 yield from water ice films under 1.5 MeV Ne^+ irradiation at 7 K.[38,39] To test for the occurrence of radiation-induced diffusion in our case, we irradiated ice films to O_2 yield saturation at 20 and 100 K, and capped them with H_2O overlayers of varying thicknesses. These films were irradiated once more, and the O_2 yield transients were measured. If O_2 emission were strictly a surface phenomenon, the O_2 transient would resemble that of a fresh film until the overlayer is entirely removed by sputtering, whereupon the O_2 emission would quickly reach the equilibrium value of the underlying irradiated ice. If, however, O_2 emission were influenced by diffusion of trapped O_2 or precursor molecules from beneath the surface, then the O_2 transient would deviate from that of a fresh film *before* the overlayer is removed.

Figure 5 shows the O_2 yield versus irradiation fluence at 100 K for overlayers of different thicknesses deposited onto an 8500 ML film previously irradiated at 100 K to O_2 yield saturation. Total sputtering yields were approximately constant for all transients displayed in Fig. 5, since the O_2 contribution is small at 100 K. Consequently, the number of molecules removed by sputtering is proportional to irradia-

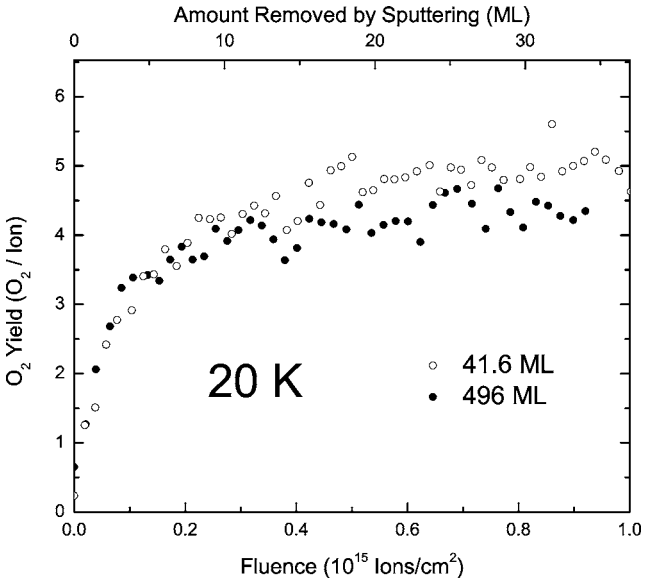

FIG. 6. Similar experiment to Fig. 5 repeated at 20 K.

tion fluence, leading to the top scale given in Fig. 5. As shown, deposition of a 376 ML overlayer restored the O_2 yield transient to that of a fresh film. However, the transients for 63.7, 37.0, and 18.2 ML overlayers were different; they followed that of a fresh film only initially. At fluences *prior* to the removal of the overlayers, the O_2 yields exceeded that of a fresh film by almost a factor of two. For instance, the O_2 yield began to surpass that of a fresh film for a 63.7 ML overlayer while a thickness of about 40 ML still remained. Therefore, the ion beam caused diffusion of species from the underlying (previously irradiated) ice through the overlayer and to the surface where they affected the O_2 yield.

We obtained different results when the experiment of Fig. 5 was repeated at 20 K. As shown in Fig. 6, deposition of a 496 ML overlayer restored the O_2 yield transient to that of a fresh film. In contrast to Fig. 5, however, the transient did not deviate significantly from that of a fresh film when the overlayer thickness was reduced to 41.6 ML. Therefore, we conclude that radiation-induced diffusion of species from the underlying ice is minor at 20 K compared to 100 K.

E. Interpretation of the results

The results reported in the preceding section demonstrate the existence of temperature-dependent radiation-induced diffusion, which is likely responsible for the differences between the O_2 yield transients at 20 and 100 K in the experiments of Figs. 2 and 3. We remark that the deposition of overlayers of any thickness caused an initially negligible O_2 yield on subsequent irradiation. This shows that the O_2 yield is determined by the state of the ice surface, since the addition of an overlayer creates a fresh surface, chemically unaltered by previous irradiation. In addition, for 37.0 and 63.7 ML overlayers at 100 K (Fig. 5), a nonzero fluence is required for the O_2 yield to overshoot that of a fresh film, which indicates that more than one incident ion is required for diffusion of species that enhance the O_2 yield from the underlying ice to the new surface. Therefore, the maximum diffusion distance d for these species is less than the overlayer thickness. The 37.0 ML overlayer is eroded to 28 ML when O_2 yield overshoot begins, so $d<28$ ML. In contrast, O_2 yield enhancement begins at zero fluence for an 18.2 ML overlayer (Fig. 5). Hence, 18 ML$<d<28$ ML at 100 K.

We now address the identity of the diffusing species. Recent models have proposed that the O_2 emission results from trapped radical or stable precursors species[20,31,32] produced by the incident ions near the ice surface. In this picture, subsurface O_2 produced down to an "escape depth" (e.g., a few monolayers) desorbs from the ice immediately as it is generated, with O_2 radiolyzed below this depth remaining trapped in the ice. Fluence-dependent O_2 emission produced by low-energy (<100 eV) electron bombardment of ices has been attributed to the accumulation and dissociation of stable precursors.[40,41] In addition, trapped hydrogen peroxide, a possible precursor, has been observed in H_2O ices after 30–800 keV ion bombardment[26,42–46] though, in contrast to the O_2 yield, the concentration of radiolytic H_2O_2 *decreases* with temperature.[43–45] Previous measurements give a saturation H_2O_2 column density η_∞ in 100 keV Ar^+ irradiated water ice of $<4\times10^{15}$ molecules/cm^2 and a destruction cross section σ_d of $\sim5.9\times10^{-14}$cm^2 above 80 K,[44] so the number of H_2O_2 molecules destroyed per incident ion is $\sigma_d\eta_\infty<236$ over the entire Ar^+ penetration depth ($\sim$500 ML). Assuming that O_2 is generated from all H_2O_2 destruction events and O_2 produced within 10 ML of the ice surface escapes,[35] we obtain an upper limit of $(10\text{ ML}/500\text{ ML})\times236=4.7$ for the number of escaping O_2 molecules produced directly by each ion from a H_2O_2 precursor. The upper limit is an overestimation since destruction of H_2O_2 leads preferentially to the production of water.[47] These considerations show that the amount of ejected O_2 that could be produced directly from H_2O_2 decomposition is insufficient to account for the O_2 yields seen at 100 K and above (see Figs. 2, 3, and 5). In addition, we can also disregard HO_2 as a precursor since its concentration in the ice is so much lower than H_2O_2 that the molecule is below detectability by infrared spectroscopy.[44]

We are thus left with two possible mechanisms for O_2 emission: (i) production from O-atom precursors and ejection by a single incident ion or (ii) ejection of trapped O_2 produced by previous incident ions. Thermal desorption of O_2 molecules, shown in Fig. 4, suggests that mechanism (ii) is preponderant. We will now demonstrate that consideration of mechanism (ii) is sufficient to explain the present results.

If mechanism (ii) is dominant, then the O_2 yield is proportional to the trapped O_2 concentration at the ice surface (see Sec. III G), where we define the "surface" to be a few monolayers deep. As the species responsible for enabling O_2 ejection, trapped O_2 is also the diffusing species we have sought to identify. So let us analyze the 20 K irradiations of Figs. 2(d) and 3(c), during which diffusion of trapped O_2 is negligible. As the ice is eroded by sputtering at 20 K, the depth distribution of trapped O_2 from prior irradiation at 130 and 100 K is not altered significantly by diffusion, and the O_2 yield reflects the depth distribution of trapped O_2. The small effect of O_2 production at 20 K can be removed by subtracting the saturation O_2 yield of $\sim$4.5 (Fig. 6) from the O_2 yields of previously irradiated films. From Figs. 2(d) and

TABLE I. Temperature dependence of processes affecting the O_2 emission and trapped O_2 depth profile. All processes increase with temperature.

	Temperatures observed
Production	All Temperatures
Thermal diffusion	$\geqslant$130 K
Radiation induced diffusion	$\geqslant$100 K
Sputtering	All Temperatures
Thermal desorption	$\geqslant$40 K[a]

[a]Thermal desorption spectra show O_2 release at 40 K when films are irradiated below this temperature. This is attributed to desorption of O_2 from the surface (Refs. 26 and 50).

3(c) we deduce that previous irradiation at 130 and 100 K produces a concentration of trapped O_2 that rises fast with depth, peaks, then gradually drops inside the film. This is illustrated schematically in Fig. 8.

The depletion of O_2 near the surface is explained by the effect of diffusion and surface removal of trapped O_2, where the probability of O_2 removal is greater than that of H_2O. This is much like the "altered layer" phenomena observed in several preferentially sputtered alloys, for which diffusion is critical.[48,49] Mindful of this, we now consider the time-dependent effects observed at 130 K, where there is simultaneous O_2 production, radiation induced diffusion, thermal diffusion, and surface removal (Table I). When irradiation is interrupted, production, sputtering, and radiation-induced diffusion cease, while thermal diffusion and thermal desorption from the surface continue (as evidenced by Fig. 4). Consequently, the O_2 depth profile and surface concentration, having equilibrated during irradiation, evolve when irradiation is terminated. When irradiation is resumed, the O_2 yield differs from that prior to the interruption because the surface O_2 concentration has changed, explaining the phenomena seen in Figs. 2(b) and 3(a).

At temperatures above 130 K, the change in surface O_2 concentration on termination of irradiation is sufficiently drastic to affect the O_2 outgassing rate. Figure 7 shows the O_2 signal versus time for a sample irradiated at 150 K. The initial O_2 "overshoot" at the start of the irradiation was due to the removal of trapped O_2 from a prior irradiation at 100 K. Of greater interest, however, is the O_2 emission after termination of the irradiation, which rose, peaked, and then dropped within ~5 min. This is in agreement with the expected evolution of the surface O_2 concentration for fast thermal diffusion and desorption of trapped O_2. When removal by sputtering ceases, diffusing O_2 from beneath the depletion region rapidly accumulates at the surface. As the surface concentration rises, so does the rate of O_2 desorption from the surface, thus accounting for the observed increase in oxygen outgassing. Eventually, O_2 is depleted and O_2 outgassing drops.

Next, we analyze in greater detail the O_2 yield transients for the overlayer experiments of Fig. 5. Films irradiated to O_2 yield saturation have an O_2 depth profile like that shown schematically in Fig. 8. The profile remains unchanged at 100 K when irradiation is stopped since thermal diffusion is

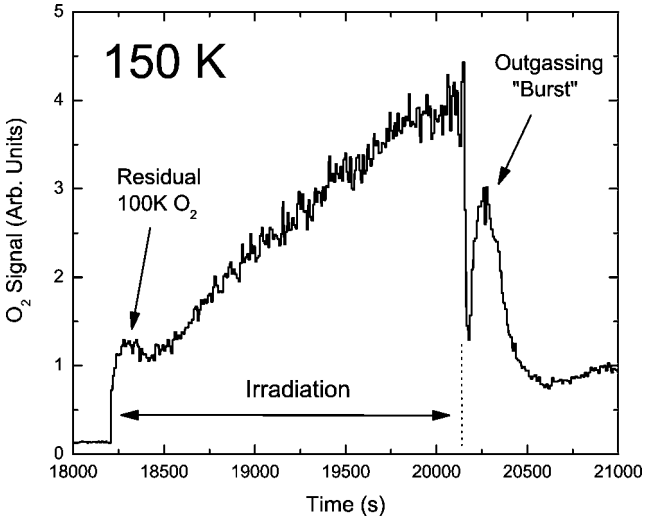

FIG. 7. O_2 signal at mass spectrometer versus time for 150 K film, previously irradiated to saturation at 100 K.

negligible at this temperature. However, if an overlayer is deposited over the O_2 saturated ice, and irradiation is resumed, the concentration of O_2 in the underlying ice is no longer limited by depletion at a nearby surface. Consequently, as additional O_2 is produced, the O_2 concentration in the underlying ice can exceed the normal saturation level. This "excess" O_2 diffuses through the overlayer and is sputtered from the surface, contributing additional O_2 to the sputtered flux. When the overlayer is removed, surface depletion is again important. Therefore, the depth profile gradually drops to that of a normal, saturated 100 K ice, and this drop is reflected in the O_2 yield.

F. Thermal diffusion and radiation damage

Figures 2(b) and 3(a) show that the O_2 yields of films of different history, irradiated at 130 K, are affected differently by interruptions in irradiation. The reduction in the O_2 yield of Fig. 2(b) indicates a drop in surface O_2 concentration

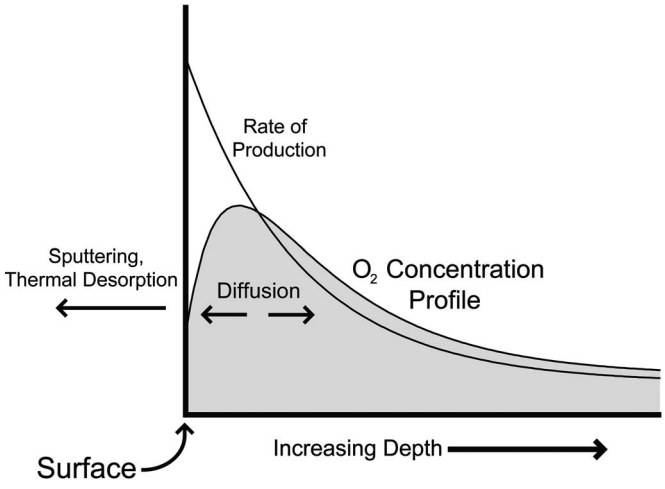

FIG. 8. Schematic illustrating the O_2 concentration versus depth and the processes that determine the depth profile.

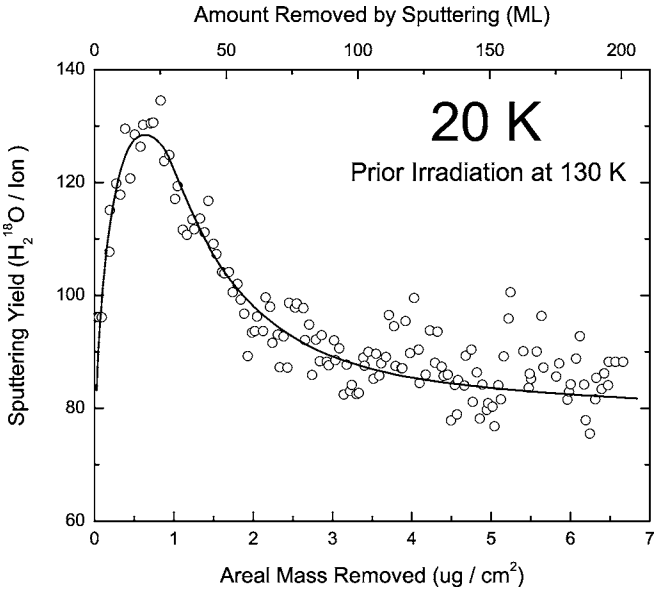

FIG. 9. Total sputtering yield versus areal mass removed at 20 K for a film previously irradiated to saturation at 130 K. Number of ML (monolayers) removed is calculated in terms of $H_2{}^{18}O$ molecular masses.

during the interruption, whereas the enhancement of Fig. 3(a) indicates an increase in the surface concentration. This can result if the rate of thermal diffusion is greater in Fig. 3(a) than Fig. 2(b), as this will transport O_2 to the surface faster than thermal desorption can remove it. The only difference between Figs. 2 and 3 is the initial 100 K irradiation. It appears, therefore, that ion irradiation at 100 K alters the films in a way that persists at 130 K and inhibits thermal diffusion of O_2 at this temperature. This is explained by the production of damage and defects by irradiation at 100 K that trap diffusing O_2 when the film is taken to 130 K. Trap production is therefore temperature dependent, being greater at 100 K than 130 K.

G. Oxygen concentration

To acquire more quantitative information on the trapped oxygen concentration, we simplified the experiments. A film was first irradiated at 130 K to O_2 yield saturation and then cooled to 20 K for a second irradiation to extract the O_2 depth profile. The result is shown in Fig. 9, where the total sputtering yield as measured with the microbalance is plotted versus areal mass and the number of monolayers removed by sputtering. The penetration depth of 100 keV Ar^+, incident at 45 deg in water ice, is ~500 ML, and the electronic energy deposition drops by only ~15% over the depth plotted in Fig. 9.[34] Yet Fig. 9 indicates that the O_2 concentration decreases fast with depth (beyond the ~20 ML thick depletion region), suggesting that O_2 is produced most efficiently very close to the ice surface. This is attributed to the preferential loss of hydrogen from the near surface region, which favors the production of oxygen rich species,[20] including O_2. The initial hydrogen depletion is reflected in the data of Reimann *et al.*, which showed a nonzero D_2 yield at zero fluence, in contrast to the initially negligible O_2 yield, when a fresh D_2O film was irradiated with 1.5 MeV Ne^+ at 10 K.[14] The D_2 yield was nearly constant above a fluence of $\sim 1 \times 10^{14}$ Ne^+/cm^2, which is much lower than the fluence for O_2 yield saturation in Reimann's experiments and in the results reported here.

We can understand the effect of hydrogen loss by examining the reactions leading to O_2 formation from the H_2O dissociation products. This process starts with excitation or ionization of H_2O by the projectile or secondary electrons, which causes decomposition into OH and H by the following reactions:

$$H_2O^* \rightarrow OH + H. \tag{2}$$

Or through the ionic channel

$$H_2O^+ + e^- + H_2O \rightarrow H_3O^+ + OH + e^-, \tag{3}$$

$$e^- + H_2O \rightarrow OH^- + H, \tag{4}$$

$$OH^- + H_3O^+ \rightarrow 2H_2O. \tag{5}$$

The H and OH radicals react to form H_2O, H_2, and H_2O_2

$$H + H \rightarrow H_2, \tag{6}$$

$$OH + H_2 \rightarrow H_2O + H, \tag{7}$$

$$OH + H \rightarrow H_2O, \tag{8}$$

$$OH + OH \rightarrow H_2O_2. \tag{9}$$

Alternatively, an additional incident ion X can dissociate the hydroxyl, producing O atoms

$$X + OH \rightarrow OH^* \rightarrow O + H. \tag{10}$$

Direct production of O atoms from H_2O is also possible

$$H_2O^* \rightarrow O + H_2. \tag{11}$$

However, the removal of one hydrogen atom from the parent molecule, as in reaction (10), should be much more likely than the removal of two, as in reaction (11). Therefore, variations in the trapped hydroxyl concentration will strongly affect the production of O atoms. This in turn impacts O_2 production, since O_2 is produced by the reaction of O atoms:

$$O + O \rightarrow O_2. \tag{12}$$

Trapped or diffusing H and H_2 limit the hydroxyl concentration by reactions (7) and (8). However, hydrogen can diffuse and escape from the ice surface in the form of H_2 prior to reacting with the hydroxyl radicals, resulting in higher OH concentrations in the near surface region. Consequently, O_2 production by reactions (10) and (12) is enhanced near the surface. Moreover, O_2 destruction by additional ions is suppressed in this region, since the following reactions of O atoms with H or H_2 are less likely to precede O atom recombination

$$H + O \rightarrow OH, \tag{13}$$

$$H_2 + O \rightarrow H_2O. \tag{14}$$

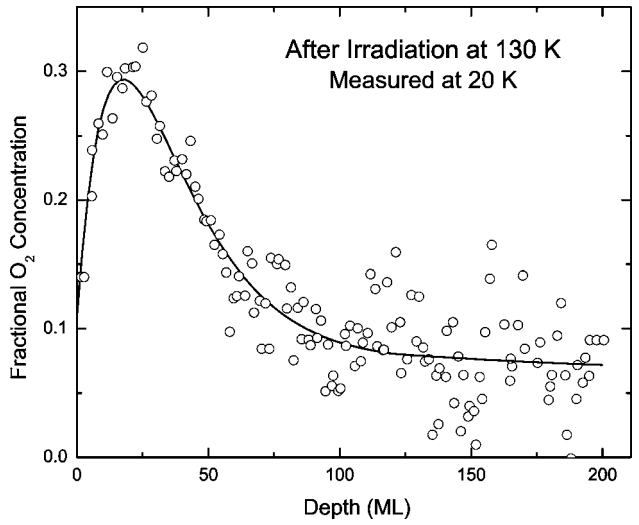

FIG. 10. O_2 concentration versus depth (in monolayers) derived from data of Fig. 9 using Eq. (15).

We can estimate the fractional O_2 concentration from the total sputtering yield of Fig. 9. Since O_2 and H_2O molecules are sputtered with different probabilities, their concentrations at the surface (as defined earlier) rapidly equilibrate on commencement of irradiation so that $Y_{H_2O}/Y_{O_2}=N_{H_2O}/N_{O_2}$, where Y_i and N_i denote the yield and *initial* number density of molecule i at the surface, respectively.[18] This expression may be rewritten in terms of the total sputtering yield Y_{tot} to give C_{O_2}, the fractional concentration of O_2

$$C_{O_2}=\frac{N_{O_2}}{N_{H_2O}+N_{O_2}}=\frac{Y_{O_2}}{Y_{H_2O}+Y_{O_2}}$$

where

$$Y_{O_2}=\frac{M_{H_2O}}{M_{O_2}}(Y_{tot}-Y_{H_2O})-Y_{20\ K}. \quad (15)$$

M_i is the molecular mass of molecule i and $Y_{20\ K}$ is the yield for O_2 produced at 20 K. As shown in Fig. 1, the total sputtering yield for a fresh 20 K film is ~70, from which $M_{H_2O}Y_{20\ K}/M_{O_2}$ can be subtracted to give $Y_{H_2O}=67.5$. Therefore, we use $Y_{H_2O}=67.5$, $M_{H_2O}=20$ amu (for $H_2{}^{18}O$), $M_{O_2}=36$ amu, and $Y_{20\ K}=4.5$ (Fig. 6) in Eq. (15) to obtain the fractional O_2 concentration versus depth from the Y_{tot} data of Fig. 9. The results are given in Fig. 10, which shows that a film irradiated to O_2 yield saturation at 130 K contains ~12% O_2 at the surface, and ~29% O_2 at ~20 ML below the surface, with the concentration dropping with depth thereafter.

Irradiation at lower temperatures produces far less O_2. When films are irradiated at 100 K, for instance, and again at 20 K to obtain a depth profile, a small O_2 emission peak is observed with the mass spectrometer, but the O_2 yield is insufficient to produce any noticeable change in the total sputtering yield. This implies a peak oxygen concentration less than 5%.

IV. CONCLUSIONS

Two experimental findings, the dependence of sputtering of O_2 on the irradiation history of the ice, and on thin surface overlayers, allowed us to make progress in the road to understanding one of the most basic problems in radiolysis. We conclude that O_2 is formed in the projectile track by a recombination of radicals, then traps, diffuses, and is ejected from the solid by sputtering or thermal desorption. The details of the processes in the ice have not yet been worked out but we have demonstrated the importance of radiation-induced diffusion, and the relative unimportance of hydrogen peroxide as a precursor for molecular oxygen formation. In addition, we showed that the depth profile of the trapped O_2 concentration can be determined by irradiation at low temperatures (e.g., 20 K), where diffusion effects are minimal.

ACKNOWLEDGMENTS

This research was supported by NSF Astronomy and NASA's Cassini and Planetary Atmospheres programs.

[1] W. L. Brown, L. J. Lanzerotti, J. M. Poate, and W. M. Augustyniak, Phys. Rev. Lett. **40**, 1027 (1978).
[2] P. Sigmund, Phys. Rev. **184**, 383 (1969).
[3] P. Sigmund, in *Sputtering by Particle Bombardment I*, edited by R. Behrisch (Springer Verlag, Berlin 1981).
[4] W. L. Brown, W. M. Augustyniak, E. Brody, B. Cooper, L. J. Lanzerotti, A. Ramirez, R. Evatt, and R. E. Johnson, Nucl. Instrum. Methods **170**, 321 (1980).
[5] W. L. Brown, W. M. Augustyniak, L. J. Lanzerotti, R. E. Johnson, and R. Evatt, Phys. Rev. Lett. **45**, 1632 (1980).
[6] W. L. Brown, W. M. Augustyniak, E. Simmons, K. J. Marcantonio, L. J. Lanzerotti, R. E. Johnson, J. W. Boring, C. T. Reimann, G. Foti, and V. Pirronello, Nucl. Instrum. Methods Phys. Res. **198**, 1 (1982).
[7] J. W. Spinks, and R. J. Woods, *An Introduction to Radiation Chemistry* (Wiley, New York, 1990).
[8] R. A. Haring, A. Haring, F. S. Klein, A. C. Kummel, and A. E. De Vries, Nucl. Instrum. Methods Phys. Res. **211**, 529 (1983).
[9] D. B. Chrisey, J. W. Boring, J. A. Phipps, R. E. Johnson, and W. L. Brown, Nucl. Instrum. Methods Phys. Res. B **13**, 360 (1986).
[10] D. E. David, and J. Michl, Prog. Solid State Chem. **19**, 283 (1989).
[11] J. Schou, Nucl. Instrum. Methods Phys. Res. B **27**, 188 (1987).
[12] J. W. Boring, R. E. Johnson, C. T. Reimann, J. W. Garret, W. L. Brown, and K. J. Marcantonio, Nucl. Instrum. Methods Phys. Res. **218**, 707 (1983).
[13] G. Ciavola, G. Foti, L. Torrosi, V. Pirronello, and G. Strazzulla, Radiat. Eff. **65**, 167 (1982).

[14] C. T. Reimann, J. W. Boring, R. E. Johnson, J. W. Garrett, K. R. Farmer, W. L. Brown, K. J Marcantonio, and W. M. Augustyniak, Surf. Sci. **147**, 227 (1984).
[15] A. Bar-Nun, G. Herman, M. L. Rappaport, and Yu. Mekler, Surf. Sci. **150**, 143 (1985).
[16] D. T. Hall, D. F. Strobel, P. D. Feldman, M. A. McGrath, and H. A. Weaver, Nature (London) **373**, 677 (1995).
[17] R. E. Johnson, L. J. Lanzerotti, and W. L. Brown, Nucl. Instrum. Methods Phys. Res. **198**, 147 (1982).
[18] R. E. Johnson, *Energetic Charged-Particle Interactions with Atmospheres and Surfaces* (Springer-Verlag, New York 1990).
[19] M. Shi, R. A. Baragiola, D. E. Grosjean, R. E. Johnson, S. Jurac, and J. Schou, J. Geophys. Res. **100**, 26387 (1995).
[20] R. E. Johnson, T. I. Quickenden, P. D. Cooper, A. J. McKinley, and C. G. Freeman, Astrobiology **3**, 823 (2003).
[21] D. T. Hall, P. D. Feldman, M. A. McGrath, and D. F. Strobel, Astrophys. J. **499**, 475 (1998).
[22] L. J. Lanzerotti, C. G. Maclennan, W. L. Brown, R. E. Johnson, L. A. Barton, C. T. Reimann, J. W. Garrett, and J. W. Boring, J. Geophys. Res. **88**, 8765 (1983).
[23] D. T. Young and the Cassini Plasma Science Team, Science **307**, 1262 (2005).
[24] R. L. Tokar, R. E. Johnson, M. F. Thomsen, D. M. Delapp, R. A. Baragiola, M. F. Francis, D. B. Reisenfeld, B. A. Fish, D. T. Young, F. J. Crary, A. J. Coates, D. A. Gurnett, W. S. Kurth, Geophys. Res. Lett. **32**, L14S04 (2005).
[25] R. A. Baragiola, C. L. Atteberry, C. A. Dukes, M. Fama, and B. D. Teolis, Nucl. Instrum. Methods Phys. Res. B **193**, 720 (2002).
[26] D. A. Bahr, M. Fama, R. A. Vidal, and R. A. Baragiola, J. Geophys. Res. **106**, 33285 (2001).
[27] R. E. Johnson and J. Schou, Mat. Fys. Medd. K. Dan. Vidensk. Selsk. **43**, 403 (1993).
[28] J. R. Spencer, W. M. Calvin, Astron. J. **124**, 3400 (2002).
[29] R. E. Johnson, R. W. Carlson, J. F. Cooper, C. Paranicus, M. H. Moore, and M. C. Wong, *Jupiter: The Planet, Satellites and Magnetosphere*, edited by F. Bagenal, T. Dowling, and W. McKinnon (Cambridge University Press, Cambridge, UK 2004).
[30] J. R. Spencer, W. M. Calvin, and M. J. Person, J. Geophys. Res. **100**, 19049 (1995).
[31] P. D. Cooper, R. E. Johnson, and T. I Quickenden, Icarus **166**, 444 (2003).
[32] R. E. Johnson and T. I. Quickenden, J. Geophys. Res. **102**, 10985 (1997).
[33] A. Oliva-Florio, R. A. Baragiola, M. M. Jakas, E. V. Alonso, and J. Ferron, Phys. Rev. B **35**, 2198 (1987).
[34] TRIM03 program available from http://www.srim.org/SRIM/SRIM2003.htm [based on J. F. Ziegler, J. P. Biersack, and U. Littmark, *The Stopping and Range of Ions in Solids* (Pergamon Press, New York, 1985)].
[35] R. A. Vidal, B. D. Teolis, and R. A. Baragiola, Surf. Sci. **588**, 1 (2005).
[36] R. A. Baragiola, R. A. Vidal, W. Svendsen, J. Shou, M. Shi, D. A. Bahr, and C. L. Atteberrry, Nucl. Instrum. Methods Phys. Res. B **209**, 294 (2003).
[37] R. A. Baragiola, and D. A. Bahr, J. Geophys. Res. **103**, 25865 (1998).
[38] J. Benit, and W. L. Brown, Nucl. Instrum. Methods Phys. Res. B **46**, 448 (1990).
[39] J. Benit, W. L. Brown, and C. G. Maclennan, Nucl. Instrum. Methods Phys. Res. B **59/60**, 68 (1991).
[40] M. T. Sieger, W. C. Simpson, and T. M. Orlando, Nature (London) **394**, 554 (1998).
[41] T. M. Orlando and M. T. Sieger, Surf. Sci. **528**, 1 (2003).
[42] R. A. Baragiola, M. J. Loeffler, U. Raut, R. A. Vidal, and C. D. Wilson, Radiat. Phys. Chem. **72**, 187 (2005).
[43] M. H. Moore, and R. L. Hudson, Icarus **145**, 282 (2000).
[44] M. J. Loeffler, U. Raut, R. A. Vidal, R. A. Baragiola, and R. W. Carlson, Icarus **180**, 265 (2005).
[45] O. Gomis, G. Leto, and G. Strazzulla, Astron. Astrophys. **420**, 405 (2004).
[46] O. Gomis, M. A. Satorre, G. Strazzulla, and G. Leto, Planet. Space Sci. **52**, 371 (2004).
[47] M. J. Loeffler, B. D. Teolis, and R. A. Baragiola (unpublished).
[48] G. Betz, and G. K. Wehner, in *Sputtering by Particle Bombardment II*, edited by R. Behrisch (Springer Verlag, Berlin, 1983).
[49] H. H. Anderson, in *Ion Implantation and Beam Processing*, edited by J. S. Williams and J. M. Poate (Academic Press, New York, 1984).
[50] R. A. Vidal, D. Bahr, R. A. Baragiola, and M. Peters, Science **276**, 1839 (1997).